Maejo International Journal of Energy and Environmental Communication

Journal homepage: https://ph02.tci-thaijo.org/index.php/MIJEEC

ARTICLE

Synthesis and characterization of TiO_2 and palm oil fiber ash hybrid photocatalysts for seawater pretreatment

Abdulkarim Abdulrahman Mohamed Suliman[1,3*], Ruzinah Isha[1*], Mazrul Nizam Abu Seman[1], Abdul Latif Ahmad[2]

[1] Faculty of Engineering Technology of Chemical and Process, Universiti Malaysia Pahang, Lebuhraya Tun Razak, 23600 Kuantan Pahang, Malaysia
[2] School of Chemical Engineering, Universiti Sains Malaysia, Engineering Campus, 14300 Nibong Tebal, Pulau Pinang, Malaysia
[3] Sirte Oil Company for Production, Manufacturing of Oil & Gas, Marsa al Brega, Libya

ARTICLEINFO

Article history:
Received 7 August 2020
Received in revised form
23 August 2020
Accepted 06 September 2020

Keywords:
Desalination
Palm oil fiber ash
Photocatalyst
Seawater
Titanium dioxide

ABSTRACT

Titanium dioxide (TiO_2) has been used in various applications such as air purification, water purification, and photoelectrochemical conversion systems. However, developing advanced materials with enhanced performance for catalytic applications, especially water treatment, is highly required. This work aims to study the effect of (TiO_2) photocatalyst in pretreatment seawater desalination. The catalyst with a mass ratio of TiO_2: palm oil fibre ash (POFA) at 0:100, 40:60, 60:40, and 100:0 was synthesized via wet impregnation. The catalyst was calcined at 500 ℃ for four hours. The mixture of artificial seawater and catalyst at a mass ratio of photocatalyst: artificial seawater at 1:300 was put in a one-litre borosilicate photo-reactor fixed with mercury light of 350 nm for two hours with stirring at 1000 rpm. In this investigation, an evaporator was used to collect the freshwater. The fresh and spent catalysts were characterized via X-Ray Diffractogram (XRD), Nitrogen physisorption analysis, Diffuse Reflectance Spectrometer (DRS), Scanning Electron Microscopy (SEM), and Energy Dispersive X-Ray Spectroscopy (EDX). The catalyst with Ti: palm oil fibre ash (POFA) at 40:60 and 60:40 can reduce the COD at 45 % and 41%, respectively. As more OPFA was added into the hybrid TiO_2 catalyst, there has been a change in the properties of seawater due to the use of special evaporators, especially EC and TDS. It can be deduced that the hybrid TiO_2 photocatalyst synthesized with OPFA has vast potential to treat seawater.

1. Introduction

There are mainly three categories of water sources for any water supply: drinking, domestic purposes, agriculture, and industrial uses. These categories include rainwater, groundwater, and surface water. Even though the water covers 75% of the earth's surface, most of this water is salty seawater. Seawater contains many contaminants such as dissolved organic matter and other pollutants that come from industries and domestic buildings close to the sea and discharge their wastes into seawater (Kamble, 2014; Bhuyar et al., 2020). Moreover, oil spilt from tankers and lines for transporting crude oil (Cozzi et al., 2014). According to World

*Corresponding authors.
E-mail address: ruzinah@ump.edu.my (Ruzinah Isha); Abdulkrim@sirteoil.com.ly (Abdulkarim Abdulrahman Mohamed Suliman)

Health Organization (WHO), 80% of diseases are caused by water, whereas 80% of the world's population is facing threats to water security (Ahmed & Ismail, 2018), and 3.1% of deaths are due to unhealthy and poor water quality (Pawari & Gawande, 2015). In many countries, drinking water standards do not meet WHO standards (Khan et al., 2013). However, despite projections that world urban populations increase to nearly 5 billion by 2030 (Capitanescu et al., 2017).

Due to the scarcity of fresh drinkable water, the desalination of seawater sources has emerged as a prominent approach to meet the demand for clean potable water (Loucks & Van Beek, 2017; Bhuyar et al., 2019a). However, techniques for desalination require a high amount of operational energy to convert the seawater to drinking water, such as membrane and thermal desalination processes (Elimelech & Phillip, 2011). In addition, the fouling of the membrane and the pipeline blocking due to the deposition of the contaminants and suspended solids during the desalination process are two of the most critical problems that increase the operational cost of these methods. (Yuan, 2017).

Many investigations seek to develop desalination processes by reducing energy consumption (Kan et al., 2016). The seawater pretreatment using a photocatalytic method is one of the promising approaches to degrade the pollutants by the photoreaction technique. In this method, the semiconductor materials have been used as photocatalytic (Kamboj & Dhir, 2009; Ahmad, et al., 2020). Semiconductor materials can enhance photocatalytic reactions by providing charge carriers represented in electrons and holes after irradiation by photons from light sources. (Sarina et al., 2013).

Moreover, these materials have excellent properties like low cost, resistance to photosynthesis, and ability to absorb visible or UV light (Al-Rasheed, 2005). Titanium dioxide (TiO_2), also known as titanium (IV) oxide or titania, is the most commonly used catalyst in photocatalysis. The advantages of TiO_2 are such as good activity (the photogenerated holes are highly oxidizing), high physical and chemical stability both in acidic and basic conditions. In addition to that, TiO_2 are nontoxicity and resistant to corrosion, commercial availability, and inexpensiveness (Carp et al., 2004; Huang et al., 1999; Ohtani et al., 2010). The commercially available photocatalysts have poor degradation efficiency and a low utilization rate of visible light. So, to improve the photocatalysts activity, the Surface and Bandgap modification (Rehman et al., 2009). In photocatalytic desalination techniques, the photoreactivity of the TiO_2 can be enhanced by combining it with high surface area supported materials and which can act as an absorbent.

Several hybrid materials have a porous structure to develop adsorption and photocatalysis for water treatment (Guo et al., 2009). In this regard, palm oil fibre ash (POFA) recently attracted research interest from different Malaysian research institutions to take advantage of some features such as porous structure, adsorption, and the low cost of POFA. More than 5.1 million hectares of farmland are exploited in Malaysia to plantation oil palm and produce about 18.8 million tons of crude palm oil per year (Ng et al., 2016; Bhuyar, et al., 2019b). Besides, the large amount of solid waste such as palm oil fibre ash (POFA), oil palm trunks (OPT), oil palm fronds (OPF), empty fruit bunches (EFB), palm pressed fibres (PPF), and palm oil mill effluent (POME) has been generating in the palm oil industries (Tangchirapat et al., 2007; Nithin et al., 2020). OPFA is one of the primary non-toxic waste sources and generally producing from the-product thermal power generation plants (Demirbas, 2005). Oil palm ash (OPFA) generates from a palm oil mill which is highly biomass dispersive. OPFA is one of the significant waste sources. It is a by-product of thermal power generation plants. It is non-toxic, cheap OPFA may be suitable (Yu, 2004). Biomass wastes are burnt directly in power plants to raise steam, which later expanded through a turbo-alternator to generate electricity (Demirbas, 2005; Yaman, 2004). Physically, POFA is greyish in the cooler and becomes dark with increasing proportions of unburned carbon (Rusbintardjo et al., 2013). POFA has also emerged as an ideal adsorbent in the wastewater treatment processes and an air purifier in cleaning atmospheric contaminants. Besides, many studies seek to benefit from the waste and use it in many environmental applications; for example, POFA in catalysis as support of TiO_2 photocatalyst is interestingly investigated. The combination of TiO_2 and POFA may degrade seawater contamination, whereas OPFA also acts as an adsorbent for some pollutants and eliminates the water salinity (Ahmad et al., 2012). Therefore, this study has investigated the effects of the different mass ratios between the TiO_2 and ash as a hybrid photocatalysis to reduce the salt concentration in seawater and degrade contaminates by using the light wavelength of 365 nm, which can be achieved by modifying the properties of the particles through the surface treatment or increase in crystallite size and changes in the microstructure.

2. Materials and Methods

2.1. Material Preparation

OPFA was obtained from Felda Lepar Hilir 3 palm oil mill, Gambang, Kuantan, Pahang, and it was the waste produced through the burning of palm oil fibre in boilers used to generate electricity. The artificial seawater (ASW) was used either with an evaporator or without the evaporator. ASW was prepared, the stock solution was made first by dissolving the 1 g of Humic acid (HA) in 1 L of deionized water with 2 to 3 pellets of NaOH. Then add 15 ml of stock solution to 1L of deionized water with 30 g of NaCl to prepare one litre of ASW. The ingredients were mixed well, and the magnetic terrier was used. Titanium Dioxide (TiO_2) with a purity of more than 99 % from Sigma-Aldrich.

2.2. Catalyst Preparation

Hybrid titanium and palm oil fibre ash (Ti:Ash) photocatalysts were prepared by Wetness Impregnation techniques. In this investigation, a different mass ratio of TiO_2 with POFA was used (40:60 and 60:40). As a first step, TiO_2 and POFA were mixed in deionized water and stirred at 80 °C for four hours, then drying overnight at 100 °C in the oven, followed by a calcination step at 500 °C in the furnace for four hours also. Finally, the catalyst was

crushed and sieved to the size of < 125 μm to homogenize the size of the catalyst.

2.3. Catalyst Characterization

Ti:Ash's fresh and spent TiO2, Ash, and photocatalysts were characterized by their specific surface area, pore-volume, and pore size by N_2 adsorption-desorption using Micro-merits. Before the analysis, the catalyst was degassing at 200˚C for 6 h., and the crystal structure was analyzed by using the X-ray powder diffraction (XRD) equipped with Cu Kα source with a wavelength (λ) of 1.5405 Å at 15 mA and 30 kV and scanning in the 2θ range of 10°-80° at 4° min-1 via Rigaku Miniflex II. Surface morphology tested by Scanning Electron Microscopy (SEM). Meanwhile, elements analysis was identified by Energy Dispersive X-Ray Spectroscopy (EDX) via QUANTA 450 at the central laboratory, University Malaysia Pahang UMP.

2.4. Photocatalytic Reactor Setup

Artificial seawater photoreaction was conducted in a borosilicate reactor with a one-litre capacity under UV light irradiation, as shown in fig 1. The photoreaction of artificial seawater was conducted in a borosilicate reactor with a one-litre capacity under UV light irradiation. In this investigation, the experiment was carried out with two different modules. The first one, the borosilicate reactor, was covered by a flat roof, and no freshwater was collected in this state. In the second design, a new pyramidal cover with a square base was used to condense and collect freshwater instead of a vacuum pump and condenser to collect the distilled freshwater.

The pyramidal design consists of two parts which are the pyramid roof with 45° for each side and a square base with dimensions (18cm * 18cm). The square part is open from the bottom by an inner diameter of 10.12 cm, which equals the reactor diameter. The weight of these two parts is 1.16 kg, to know the amount of freshwater produced by the difference in pyramid weight before and after each run. The light source was a UV lamp with a wavelength of 365nm was installed next to the reactor at a distance of 0.03m. Each run was performed for 2 h and simultaneously stirred at 400 rpm to ensure the complete mixing of the solution. In addition, the ratio of catalyst to the seawater sample was. 1:300 in the final solution. Thus, about 2.7 g of the sample was added to the 800 ml of artificial seawater (ASW). After the experiment was carried out, the catalyst was filtered out from all samples.

The quality of water was analyzed before and after the run. The EC, COD, PH, and Turbidity of the water were determined. The (Hach Sension + 150 mm) was used to determine the pH, conductivity (EC), and Total dissolved solids (TDS) of the seawater. The COD digestion Reagent Vial High Range (435 COD HR) was used to determine the organic compound in the artificial seawater before and after each run. Meanwhile, the turbidity of seawater was measured by the Turbidity meter Hach 2100 model before and after each run. Every measurement was repeated three times, and the average value was taken as the experiment's outcome.

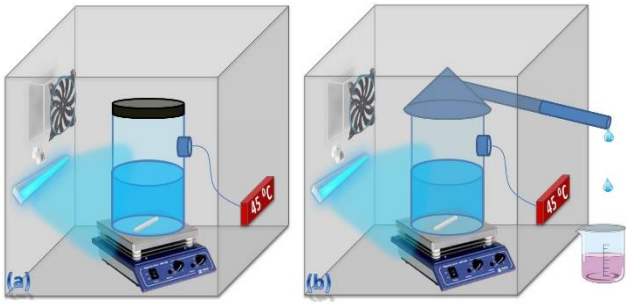

Fig. 1 Schematic diagram of batch photocatalytic reactor set up, (a) a photoreactor with an evaporator (b) a photoreactor without an evaporator.

3. Results and Discussion

3.1. Surface Area Analysis

Table 1 shows the results of BET analysis for the surface area, pore-volume, and pore size of fresh and used photocatalysts of TiO_2, Ash, and different mixtures ratios of Ti:Ash. The pore diameter in the range of 5.30 nm to 34.21 nm indicated that all fresh and used photocatalysts exhibit the mesoporous nature of materials. Surprisingly, the BET surface area of bare TiO_2 was increased to double after the reaction from 5.7 m^2/g to 10.1 m^2/g. Moreover, the same pattern of increase can be observed for hybrid catalysts from 3.9 m^2/g to 6.1 m^2/g and 4.3 m^2/g to 11 m^2/g of 40:60 and 60:40, respectively. At the same time, the surface area of pure oil palm fibre ash was decreased from 18.1 m^2/g to 12.9 m^2/g. The increase of the surface area of TiO_2 in the photocatalytic process is related to the production of species reactive in the solution (Andayani & Bagyo, 2011). W. E. Kan claims that the TiO_2 has an inflation character off in the water, which leads to an increase in the surface area of the catalyst after the reaction (Kan et al., 2016). However, the pore volume of bare TiO_2 was decreased from 5.6×10^{-2} cm^3/g to 4.2×10^{-2} cm^3/g, as well as the Ti:Ash 0:100, which decreased from 2×10^{-2} cm^3/g to 0.3×10^{-2} cm^3/g. Whereas, Ti:Ash 40:60 and 60:40 increased from 1.7×10^{-2} cm^3/g to 3.2×10^{-2} cm^3/g and 3.6×10^{-2} cm^3/g to 4.9×10^{-2} cm^3/g respectively. As shown in Table 1, the BET surface area, total pore volume, and diameter for the TiO_2 and Ash mixture photocatalysts at different ratios (40:60 and 60:40) were increased after the reaction. This increasing trend again showed the predominance of TiO_2 in the catalyst mixture, which gets inflated after interacting with the water and increases the overall catalysts' surface area. It was expected that the high values for pore size and BET surface area obtained for the TiO_2 and ash mixtures could increase the photocatalytic activity of the catalyst (Kim et al., 2007). Also, Guo et al. reported that smaller pore size was not compatible with the diffusion of the photoelectrons, which leads to a decrease in the performance

(Nichols & Smith, 2009). Moreover, the open mesoporous structure was more efficient for the photocatalytic decomposition of dye, acetone, and water (Ji et al., 2017; Katou et al., 2003; Miao et al., 2016).

Moreover, the isotherms from N_2 physisorption of Ti:Ash 40:60 and 60:40 are presented in fig. 2 (a) and (b). The isotherms showed type V isotherms with hysteresis loop according to Brunauer, Deming, Deming, and Teller (BDDT) classification, which are the typical characteristic of mesoporous materials (Wang et al., 2012). The IUPAC classification of adsorption isotherms type V represents mesoporous materials (Lowell et al., 2012; Sing, 1985).

Table 1 Physical properties of TiO_2, Ash, and Ti:Ash hybrid photocatalysts.

Catalyst the weight ratio of TiO_2:Ash (%)	Specific surface area (m^2/g)		Pore volume $\times 10^{-2}$ (cm^3/g)		Pore size (nm)	
	Before	After	Before	After	Before	After
100% TiO_2	5.7	10.1	5.6	4.2	22.2	23.2
100% Ash	18.1	12.9	2	0.3	7.1	5.3
40:60	3.9	6.1	1.7	3.2	21.5	17.4
60:40	4.3	11.0	3.6	4.9	34.2	18.1

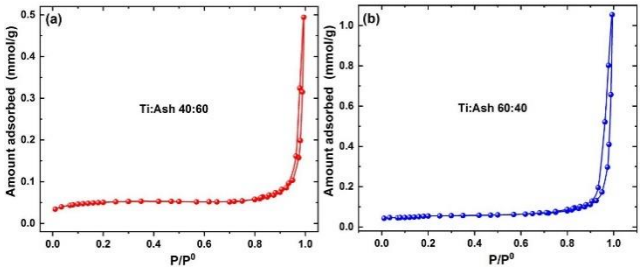

Fig. 2 Isotherms obtained from liquid N_2 physisorption test (A) Ti:Ash 40:60, (B) Ti:Ash.

3.2. Phase Identification and Structural Properties

Figures 3 (a) and (b) depict the XRD pattern of TiO_2 and palm oil fibre ash (OPFA) with different Ti:Ash weight ratios before and after testing in the hybrid photocatalytic reactor system. From the patterns in figure 3 (a), we can notice that the predominant crystal structure of the TiO_2 is anatase type. Meanwhile, the XRD patterns of ash peaks of crystalline phase of silicon oxide in hexagonal boron nitride (h-BN) form as shown in fig. 3 (a). As seen in fig. 3 (a), the sharp and high-intensity peaks appeared at 2θ of 25.728° and 27.081°, almost the same place for fresh TiO_2 and Ash, respectively. According to Sun et al., the change in the phase type in TiO_2 is related to calcination temperature. In this study, the calcination temperature was 500 °C which is less than the transformation temperature to the other kind, either rutile or brookite (Q. Sun et al., 2015). The conversion of anatase and brookite into rutile does not occur at room temperature, but both metastable phases become rutile when exposing to high heat above 700 °C (Porter et al., 1999). Wearers, E. F. Heald et al. claim that the impurities might influence the anatase to transform to another phase in the range of 600°C to 1100 °C temperatures. Maniam et al. reported that 600°C is the optimum temperature for calcification of the OPFA because a clear crystal structure and the sharp peaks were intensified, and amorphous peaks were seen at a much lower intensity (Maniam et al., 2015). The calcination treatment enhances the intensity of the few diffraction peaks, as illustrated by the crystalline phase of the catalyst, to become more regular.

On the other hand, TiO_2 and Ash show an excellent ability to absorb a salt by observing some salt peaks at the same place of 2θ at 32.5 for both spent catalysts. Moreover, other peaks appeared at 2θ of 45.948 and 35.8 for TiO_2 and Ash, respectively. Other studies have also indicated similar peaks for salts appeared between 32.20°and 45.50° for spent TiO_2 photocatalysts (Kan et al., 2016; Yalçin & Mutlu, 2012). This finding confirms that immersion TiO_2 in seawater during the reaction for two hours causing the salt particles to adsorb to TiO_2. Moreover, the salt might cause deposition on the TiO_2 surface. This idea is supported by the change in the surface area, pore size, and pore volume of spent TiO2, which is clarified in Table 1. Hexagonal boron nitride (h-BN) has been considered practical support because it displays many unique physical and chemical properties such as high chemical stability, high thermal stability, and hydrophobic character (Liu et al., 2014; Paine & Narula, 1990). Figure 3 (b) also depicts the XRD patterns for synthesized Ti:Ash photocatalysts with two different mass ratios, 40:60 and 60:40. The bare titanium sample and all photocatalysts are well crystallized, and its pattern matches well with the propagated JCPDS file. According to Ng et al., Sharp peaks indicate too high crystallinity (Ng et al., 2016). XRD diffractograms indicate that the anatase phase is predominant in Ti:Ash photocatalysts 40:60 and 60:40. Moreover, it is worth noting that neither oil palm fibre ash nor calcination temperature induces crystal phase transition of the photocatalysts, as can be observed by comparing bare TiO_2 and both hybrid photocatalysts.

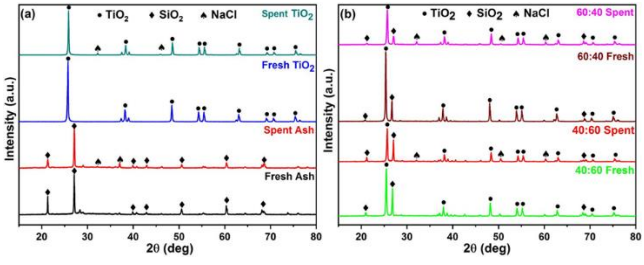

Fig. 3 XRD patterns of fresh and spent photocatalysts, (3A) fresh ash, spent ash, fresh TiO_2, and spent TiO_2. (3B) Fresh Ti:Ash 40:60, spent Ti:Ash 40:60, fresh Ti:Ash 60:40, and spent Ti:Ash 60:40.

Through XRD analysis, both Ti:Ash photocatalysts and bare TiO_2 have the same pattern with slightly different, attributed to the excellent dispersion of TiO_2 on oil palm fibre ash. Figure 3 (b) clearly shows that peaks of NaCl for Ti:Ash 60:40 and 40:60, both share the same peaks profile which is observed at 2θ of 32.1°, 51.26°, and 60.64° with a relatively better appearance for Ti:Ash 60:40 photocatalyst which indicating a good absorption capability comparing to Ti:Ash 40:60 photocatalyst. From fig. 3 (b), it is

possible to observe the presence of the characteristic peaks of the crystalline phase of quartz (SiO_2) in both photocatalysts 60:40 and 40:60 which provided by oil palm fibre ash (OPFA) between 20 and 80, for both types of catalysts the clear peaks of SiO2 in h-BN form appeared at 21.33°, 26.92°, and 68.43° of 2θ. The investigation was done by Jamo et al. indicate that the silica content in OPFA might enhance the catalyst in seawater pretreatment (Jamo et al., 2013). In particular, porous BN with a high surface area exhibits a high adsorption capacity for organic pollutants (J. Li et al., 2013; Lian et al., 2012; Liu et al., 2014). Silica content in OPFA might enhance the catalyst uses in seawater pretreatment by improving absorbing characteristics. Moreover, appearance salt peaks on spent catalysts support this observation.

3.3. Optical Properties and Band Gap Calculation

The bandgap energy of TiO_2 and Ti:Ash was observed from Diffuse Reflectance Spectrometer (DRS) as shown in fig. 4. The samples were analyzed in the range of 200– 700 nm. It was noticed that the absorption edge of TiO_2 appeared at about 398 nm, corresponding to the bandgap energy of about 3.11 eV, which is by the reported literature (Asahi et al., 2000; Kaur et al., 2016; Li et al., 2009; Pal et al., 2012). The reflectance spectra were analyzed using the Kubelka-Munk relation to convert the reflectance into a Kubelka-Munk function. Bandgap energies of the samples were estimated from the variation of the Kubelka-Munk function with photon energy. Figure 4 (b) presents the Kubelka-Munk plots for the undoped and Ti:Ash samples used to determine their bandgap energy. It can be observed that the indirect bandgap slightly increased with the increase in oil palm fibre ash (OPFA) amount.

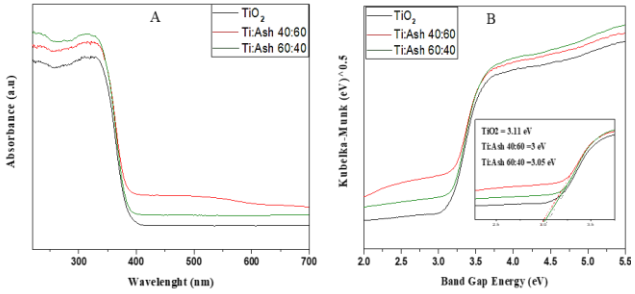

Fig. 4 (A) UV-Vis diffuse spectra of bare TiO_2 and hybrid photocatalysts of Ti:Ash 40:60 and 60:40 samples. (B) k-m plot for bandgap energy of photocatalysts.

The decrease due to metals oxides such as iron oxide in oil palm fibre ash (OPFA) may have reduced the bandgap energy. However, the estimated indirect bandgap values (3.11eV OF bare TiO_2). The bandgap of Ti:Ash was 3.05 eV and 3 eV for Ti:Ash 40:60 and 60:40, respectively. All the samples were very close to Ti:Ash's reported indirect bandgap value (Kan et al., 2016).

3.4. Morphology Analysis

SEM characterized the morphologies of as-prepared samples. The SEM images in fig. 5 (a) and (b) reveal the same synthetic structure of TiO_2 prior and after a reaction, which indicated that the TiO_2 was a stable photocatalyst (Fujishima et al., 2000; Ibhadon & Fitzpatrick, 2013; Jiang et al., 2018). Furthermore, fig. 5 (c) and (d) depicted the surface morphology of fresh and spent OPFA, respectively. It apparently can be seen that the skeleton of fresh ash consisted of irregular particles.

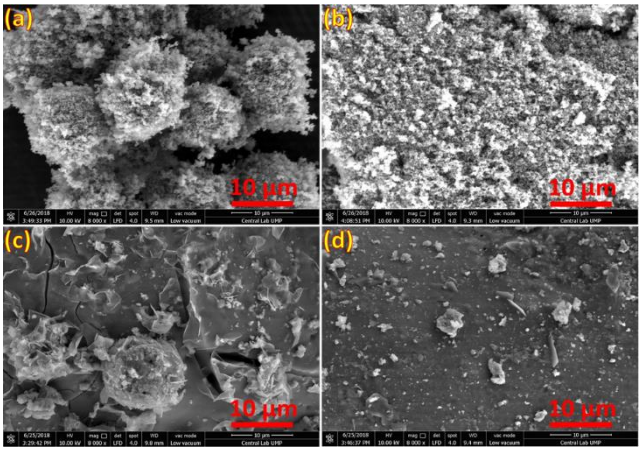

Fig. 5 SEM images of catalysts with 8000X magnification: a) the surface morphology of fresh TiO_2, b) spent TiO_2, c) fresh OPFA, d) spent OPFA.

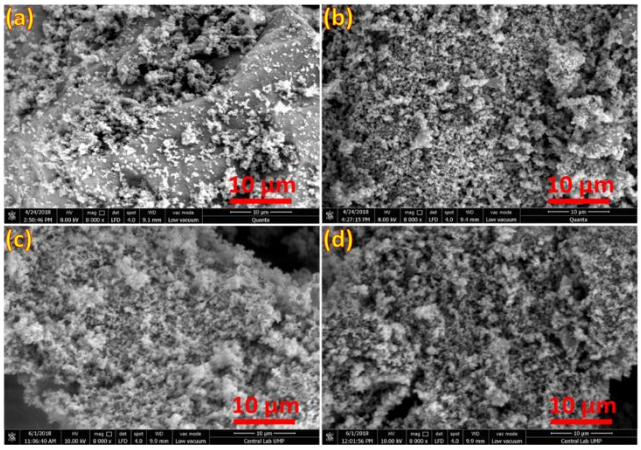

Fig. 6 SEM images of catalysts with 8000X magnification: a) fresh Ti:Ash 40:60, b) spent Ti:Ash 40:60, c) fresh Ti:Ash 60:40, d) spent Ti:Ash 60:40.

Weerana et al. (2016) reported that the skeleton of OPFA consisted of angular and irregular particles shape. Figure 5 (d) depicts the deterioration of the skeleton of POFA after the reaction. The ash structure may have deteriorated due to the dissolved some of its components into the water or reaction with the salt. On the other hand, fig. 6 (a) and (b) revealed the morphology of fresh and spent Ti:Ash 40:60. At the same time, fig. 6 (c) and (d) illustrated

fresh and spent Ti:Ash 60:40. Moreover, fig. 6 (a) and (b) show a proper distribution of TiO_2 on the OPFA surface in both fresh catalysts of Ti:Ash 40:60 and 60:40, respectively, also there are the well-dispersed spherical aggregated tiny particles of uniform diameter. In addition, the spent catalysts of Ti:Ash 40:60 and 60:40 showed the same behaviour also after testified. The TiO_2 structure did not change after the reaction, but there is rupture of OPFA that can be observed in spent catalysts illustrated in fig. 6 (b), and (c) of Ti:Ash 40:60, and 60:40 respectively. This might cause by the effect of the contact between water and POFA.

3.5. Elemental Analysis

The dispersive energy X-ray (EDX) spectrum of all catalysts is shown in fig. 7 (a) to (h). From fig.7 (e) and (g), the Ti, O, C and Si peaks are found in the fresh Ti:Ash photocatalysts spectra, which confirmed that TiO_2 existed in the matrix. The presence of Na in spent Ti:Ash photocatalysts, as illustrated in fig.7 (f) and (h) confirming that the Ti:Ash photocatalysts absorb some salt. Besides, the spectra of OPFA show the presence of C, Si, K, and Fe.

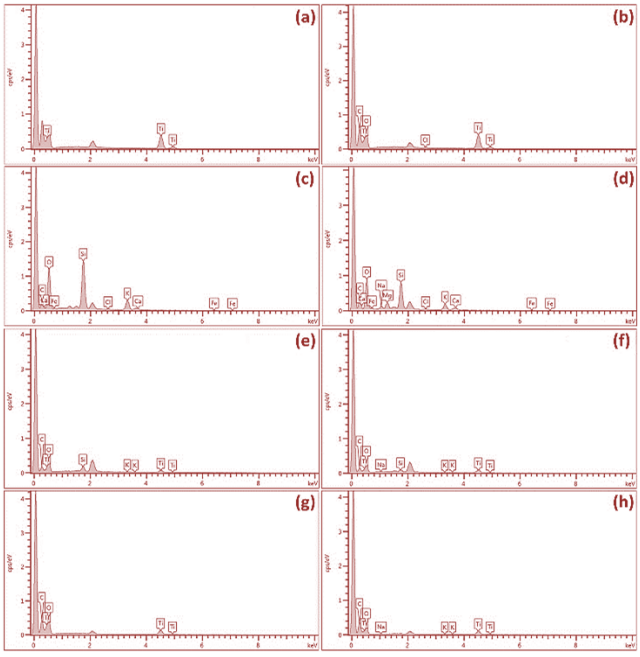

Fig. 7 EDS mapping image of all catalysts: a) fresh TiO_2, b) spent TiO_2, c) fresh OPFA, d) spent OPFA, e) fresh Ti:Ash 40:60, f) spent Ti:Ash 40:60, g) fresh Ti:Ash 60:40, h) spent Ti:Ash 60:40.

3.6. Effect of Hybrid Catalyst (Ti:Ash) on (ASW)

The parameters of seawater analyzed in this investigation were pH, COD, and turbidity. All parameters are illustrated in fig. 8 (a) to (d).

The turbidity was decreased by 51 % from 4.3 NTU to 2.1 NTU after being treated with Ti:Ash 0:100. Whereas, reduced by 47 % after used Ti:Ash 100:0, which started from 4.3 NTU to 2.26 NTU, while without catalyst, the amount of turbidity has not changed before and after testing but after using the Ti:Ash photocatalysts, the artificial seawater turbidity was decreased by 49 % from 4.03 NTU to 2.06 NTU after treated with Ti:Ash 40:60. Whereas, reduced by 41 % after used Ti:Ash 60:40, which started from 4.03 NTU to 2.36 NTU. The reduction of the water turbidity is caused by the filtration process that was carried out to separate the catalysts from samples and might be related to the degradation of Humic, as shown in fig. 8 (a). It also can be observed that the COD of Ti:Ash 100:0 reduced from 775 mg/L to 510 mg/L, which signifies up to 34 % reduction compared to Ti:Ash 0:100, which decline from 775 mg/L to 550 mg/L which was up to 2914 reduction. Whereas the seawater treated without a catalyst, the value of COD went down by 7 % only from 750 mg/L to 720 mg/L, as showing in fig. 8 (b). Sun, Liu, Liu reported the observation, and Wang (Sun et al., 2014) that titanium dioxide can adsorb and degrade water contaminates by photoreaction. In addition, OPFA reduced COD because some elements originally contained in the OPFA work as an adsorbent to adsorb the pollutants in the seawater. On the other hand, and from fig. 8 (b) also it is the sea that there is a difference in the percentage of decline where it can be noted that for Ti:Ash 60:40, the ratio was 41 % comparing to 49 % was for Ti:Ash 40:60 which might be related to TiO_2 ratio in Ti:Ash 60:40 which is more than Ti:Ash 40:60. Furthermore, fig. 8 (b) illustrates that seawater's COD reduced after treatment using Ti:Ash 40:60 decreased by up to 41 % from 775 mg/L to 460 mg/L.

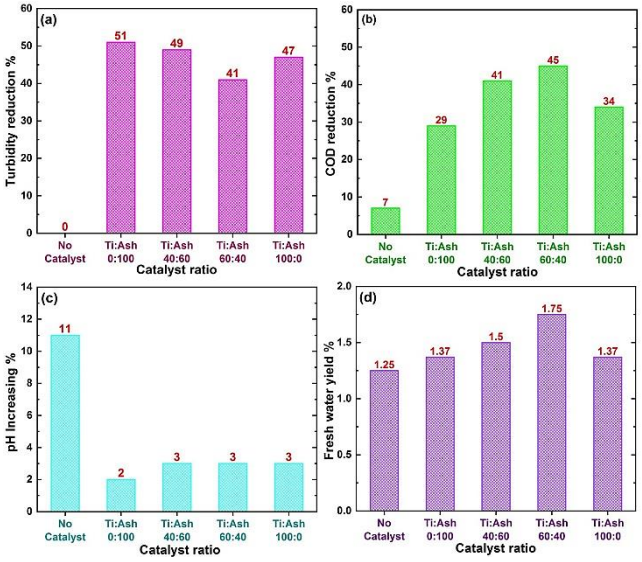

Fig. 8 All catalysts treated Analytical test of seawater: (a) Turbidity (b) COD (c) PH (d) freshwater yield.

Whereas the seawater treated by Ti:Ash 60:40 which declined from 775 mg/L to 430 mg/L, which was up to 45 % reduction as shown in fig. 8 (b). It can be deduced that the decline of the value of the chemical oxygen demanded denotes that both catalysts can reduce the organic and inorganic matter in artificial seawater, which was represented in humic acid. Bekbolet and Ozkosemen

(Bekbölet & Özkösemen, 1996) investigated that photocatalytic degradation using humic acid as a model and observed that after one hour in presence irradiation and by using 1.0 g/L of TiO_2 (P25), 40 % TOC and 75 % of the colour were removed. On the other hand, Eggins and coworkers (Eggins et al., 1997) found the irradiation of TiO_2 (P25) by a mercury lamp exhibited a very efficient reduction of humic acid concentration about 50% in 12 min. Flanders and Steenari (Olanders & Steenari, 1995) claimed that the biomass ash was rich with Ca, Si, Al, Ti, Fe, Na, Mg, K, P, and S, which can enhance the adsorbent property to remove water contaminants. The PH of artificial seawater increased by 2 % and 3 % after being treated with bare TiO_2 and palm oil fibre ash. While when treated without, the percentage of pH increasing was 11 %. The pH also increased from 6.90 to 7.11 by 3 % when Ti:Ash 40:60 was used. Besides, there was almost the exact change in seawater pH when Ti:Ash 60:40 was used, which by 3 %, as showing in fig. 8 (c). In particular, the change in pH value is might due to alkaline materials found in oil palm fibre ash (Udoetok, 2012).

3.7. TDS and EC Studies

Figures 9 (a) and (b) depict the percentage of total dissolved solids (TDS) and conductivity (EC) of seawater after using the evaporator in the hybrid photocatalytic reactor. Fig.8a reveals the total dissolved solids increased by 6 % with the same value in seawater from 27.4 mg/L to 29 mg/L after being treated with Ti:Ash 100:0 and Ti:Ash 0:100. While absent the catalyst, the TDS value was increased from 27.3 mg/L to 28.3 mg/L by 4 %, as shown in fig. 9 (a). Furthermore, the TDS of seawater increased slightly by the same percentage, which is 4 %, from 27.3 g/L to 28.26 g/L and from 27 g/L to 28.20 g/L when Ti:Ash 40:60 and Ti:Ash 60:40 was used respectively as illustrated in fig. 9 (a). On the other hand, fig. 9 (b) illustrates using an evaporator on seawater conductivity. From fig. 9 (b), the conductivity of ASW slightly increased from 42.76 mS/cm to 45.23 mS/cm and 45 mS/cm by 5 % and 6 % when treated with Ti:Ash 100:0 and Ti:Ash 0:100 respectively. Meanwhile, the EC of the sample which was treated without catalyst also increased from 42.6 mS/cm to 45.93 mS/cm around 8 %. fig. 9 (b), indicates that the conductivity of seawater which treated with Ti:Ash 40:60 increased from 43.23 mS/cm to 44.83 mS/cm. While the sample which Ti tested: Ash 60:40 also increased from 42.30 mS/cm to 44 mS/cm by the same percentage for both catalysts, which signifies up to 4 %. The increase in the parameters such as EC and TDS are related to collecting freshwater, leading to increased salt concentration.

In contrast, the increase is not significant because the TiO_2 and Ash absorb some amount of salts. The results reveal that supported photocatalysts have good pollutant adsorption properties, diffusion properties, and high photocatalytic activities (Liu et al., 2014). By contrast, without an evaporator, the percentage of TDS and EC were slightly decreased. This might be because the catalysts absorbed some contaminants besides the vapour water condensate under the reactor roof and fall again to the reactor.

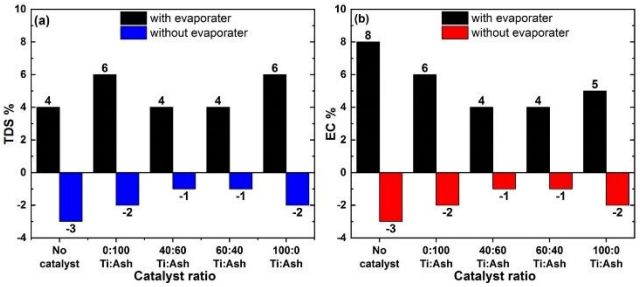

Fig. 9 Comparing TDS and EC after using evaporator in the hybrid photocatalytic system. (a) TDS, (b) EC.

It clearly can be seen in Table 2 the amount of water distilled and yield rate for seawater, which was treated without a catalyst, Ti:Ash 0:100, Ti:Ash 40:60, Ti:Ash 60:40, and Ti:Ash 0:100. Table 4, the highest freshwater production rate was achieved at 14 mL by yield (1.75 %) rate when Ti:Ash 60:40 was used. At the same time, the lowest rate was 10 mL with a production rate of up to (1.25%) when the seawater was treated without a catalyst. While Ti:Ash 40:60 produced 12 mL of freshwater with a (1.50 %) yield rate. Also, both bare TiO_2 and Ti:Ash 0:100 showed the same trend for yield rate (1.37 %) with 11ml of distillate water, as shown in figure 4f.

Table 2 Amount and Yield freshwater after testing.

	Catalyst Type				
Analytical Test	Without Catalyst	TiO_2:Ash 0:100	TiO_2:Ash 40:60	TiO_2:Ash 60: 40	TiO_2:Ash 100: 0
Amount of fresh water (Kg)	0.010	0.015	0.012	0.014	0.011
Volume of fresh water (mL)	10	11	12	14	11
Yield of fresh water (%)	1.25	1.37	1.50	1.75	1.37

4. Conclusion

In this paper, the effect of the mass ratio of titanium dioxide and oil palm fibre ash (Ti:Ash) in hybrid photocatalyst to seawater pretreatment showed that the activity of TiO_2 for seawater pretreatment was enhanced by hybrid with oil palm fibre ash (OPFA) with two different mass ratio which is Ti:Ash 40:60 and Ti:Ash 60:40. XRD pattern revealed that the hybrid of OPFA did not convert the crystalline phase of the TiO_2 besides improving the pore size and pore volume while the surface area was almost the same. In contrast, both catalysts are still working under UV because there is no change in catalysts bandgap after hybrid TiO_2 with OPFA. Moreover, both catalysts can adsorb salt (NaCl). For the chemical oxygen demand (COD) degradation test, bare TiO_2 and ash exhibited low activity under UV-light irradiation comparing to Ti:Ash 40:60 and Ti:Ash 60:40. Significant enhancement was observed when Ti:Ash 40:60 was used (45 % of COD degradation) compared to 41% of COD degradation for Ti:Ash 60:40. The seawater properties have been changed after the evaporator was used, especially EC and TDS. On the other hand,

artificial seawater (ASW) gives results closely paralleling those with natural seawater (NSW) and can be used for catalyst evaluation and the simulation of NSW. The combination of TiO_2 and oil palm fibre ash improved the photocatalytic activity and adsorbent of salt.

Declaration of competing interest

The authors declare that they have no known competing financial interests or personal relationships that could have influenced the work reported in this paper.

Acknowledgments

The authors acknowledge the support of the University Malaysia Pahang (UMP) [RDU1703242 & PGRS160331] and Sirte Oil Company for Production and Manufacturing oil and gas and Ministry of Education, Libya for a Ph.D. scholarship for one of the authors (Abdulkarim Suliman).

References

Ahmad, M.S., Cheng, C.K., Bhuyar, P., Atabani, A.E., Pugazhendhi, A., Chi, N.T.L., Witoon, T., Lim, J.W., Juan, J.C. (2020). Effect of reaction conditions on the lifetime of SAPO-34 catalysts in methanol to olefins process–A review. Fuel, 283, p.118851

Ahmad, T., Danish, M., Rafatullah, M., Ghazali, A., Sulaiman, O., Hashim, R., & Ibrahim, M. N. M. (2012). The use of date palm as a potential adsorbent for wastewater treatment: a review. Environmental Science and Pollution Research, 19(5), 1464-1484.

Ahmed, S., & Ismail, S. (2018). Water Pollution and its Sources, Effects & Management: A Case Study of Delhi.

Al-Rasheed, R. A. (2005). Water treatment by heterogeneous photocatalysis an overview. Paper presented at the 4th SWCC acquired Experience Symposium held in Jeddah.

Andayani, W., & Bagyo, A. N. (2011). TiO_2 BEADS FOR PHOTOCATALYTIC DEGRADATION OF HUMIC ACID IN PEAT WATER. Indonesian Journal of Chemistry, 11(3), 253-257.

Asahi, R., Taga, Y., Mannstadt, W., & Freeman, A. J. (2000). Electronic and optical properties of anatase TiO 2. Physical Review B, 61(11), 7459.

Bekbölet, M., & Özkösemen, G. (1996). A preliminary investigation on the photocatalytic degradation of a model humic acid. Water Science and Technology, 33(6), 189-194.

Bhuyar, P., Hong, D. D., Mandia, E., Rahim, M. H. A., Maniam, G. P., Govindan, N. (2019a). Desalination of Polymer and Chemical industrial wastewater by using green photosynthetic microalgae, Chlorella sp. Maejo Int J Energy Environ Commun, 1(3), 9–19.

Bhuyar, P., Hong, D. D., Mandia, E., Rahim, M. H. A., Maniam, G. P., Govindan, N. (2020). Salinity reduction from poly-chem-industrial wastewater by using microalgae (Chlorella sp.) collected from coastal region of peninsular Malaysia. J Bio Med Open Access.1(1):105.

Bhuyar, P., Sundararaju, S., Rahim, M. H. A., Ramaraj, R., Maniam, G. P., & Govindan, N. (2019b). Microalgae cultivation using palm oil mill effluent as growth medium for lipid production with the effect of CO_2 supply and light intensity. Biomass Conv. Bioref.1-9.

Capitanescu, F., Marvuglia, A., Benetto, E., Ahmadi, A., & Tiruta-Barna, L. (2017). Linear programming-based directed local search for expensive multi-objective optimization problems: Application to drinking water production plants. European Journal of Operational Research, 262(1), 322-334.

Carp, O., Huisman, C. L., & Reller, A. (2004). Photoinduced reactivity of titanium dioxide. Progress in solid state chemistry, 32(1-2), 33-177.

Cozzi, M., Napoli, F. D., Viccaro, M., Fagarazzi, C., & Romano, S. (2014). Ordered weight averaging multicriteria procedure and cost-effectiveness analysis for short rotation forestry in the Basilicata Region, Italy. International Journal of Global Energy Issues, 37(5-6), 282-303.

Demirbas, A. (2005). Potential applications of renewable energy sources, biomass combustion problems in boiler power systems and combustion related environmental issues. Progress in energy and combustion science, 31(2), 171-192.

Eggins, B. R., Palmer, F. L., & Byrne, J. A. (1997). Photocatalytic treatment of humic substances in drinking water. Water research, 31(5), 1223-1226.

Elimelech, M., & Phillip, W. A. (2011). The future of seawater desalination: energy, technology, and the environment. science, 333(6043), 712-717.

Fujishima, A., Rao, T. N., & Tryk, D. A. (2000). Titanium dioxide photocatalysis. Journal of photochemistry and photobiology C: Photochemistry reviews, 1(1), 1-21.

Guo, B., Shen, H., Shu, K., Zeng, Y., & Ning, W. (2009). The study of the relationship between pore structure and photocatalysis of mesoporous TiO 2. Journal of chemical sciences, 121(3), 317-321.

Huang, A., Cao, L., Chen, J., Spiess, F.-J., Suib, S. L., Obee, T. N., . . . Freihaut, J. D. (1999). Photocatalytic degradation of triethylamine on titanium oxide thin films. Journal of catalysis, 188(1), 40-47.

Ibhadon, A. O., & Fitzpatrick, P. (2013). Heterogeneous photocatalysis: recent advances and applications. Catalysts, 3(1), 189-218.

Jamo, H., Noh, M. Z., & Ahmad, Z. A. (2013). Structural analysis and surface morphology of a treated palm oil fuel ash.

Ji, J., Xu, Y., Huang, H., He, M., Liu, S., Liu, G., . . . Zhan, Y. (2017). Mesoporous TiO_2 under VUV irradiation: Enhanced photocatalytic oxidation for VOCs degradation at room temperature. Chemical Engineering Journal, 327, 490-499.

Jiang, Y., Ning, H., Tian, C., Jiang, B., Li, Q., Yan, H., . . . Fu, H. (2018). Single-crystal TiO_2 nanorods assembly for efficient and stable cocatalyst-free photocatalytic hydrogen evolution. Applied Catalysis B: Environmental, 229, 1-7.

Kamble, S. M. (2014). Water pollution and public health issues in Kolhapur city in Maharashtra. International journal of scientific and research publications, 4(1), 1-6.

Kamboj, M. L., & Dhir, A. (2009). Studies on the degradation of industrial waste water using heterogeneous photocatalysis.

Kan, W. E., Roslan, J., & Isha, R. (2016). Effect of Calcination Temperature on Performance of Photocatalytic Reactor System for Seawater Pretreatment. Bulletin of Chemical Reaction Engineering & Catalysis, 11(2), 230.

Katou, T., Lee, B., Lu, D., Kondo, J. N., Hara, M., & Domen, K. (2003). Crystallization of an ordered mesoporous Nb–Ta oxide. Angewandte Chemie International Edition, 42(21), 2382-2385.

Kaur, T., Sraw, A., Toor, A. P., & Wanchoo, R. (2016). Utilization of solar energy for the degradation of carbendazim and propiconazole by Fe doped TiO_2. Solar Energy, 125, 65-76.

Khan, N., Hussain, S. T., Saboor, A., Jamila, N., & Kim, K. S. (2013). Physicochemical investigation of the drinking water sources from Mardan, Khyber Pakhtunkhwa, Pakistan. International journal of physical sciences, 8(33), 1661-1671.

Kim, D. S., Han, S. J., & Kwak, S.-Y. (2007). Synthesis and photocatalytic activity of mesoporous TiO_2 with the surface area, crystallite size, and pore size. Journal of Colloid and Interface Science, 316(1), 85-91.

Li, J., Lin, J., Xu, X., Zhang, X., Xue, Y., Mi, J., . . . Yang, X. (2013). Porous boron nitride with a high surface area: hydrogen storage and water treatment. Nanotechnology, 24(15), 155603.

Li, L., Liu, C.-y., & Liu, Y. (2009). Study on activities of vanadium (IV/V) doped TiO_2 (R) nanorods induced by UV and visible light. Materials Chemistry and Physics, 113(2-3), 551-557.

Lian, G., Zhang, X., Zhang, S., Liu, D., Cui, D., & Wang, Q. (2012). Controlled fabrication of ultrathin-shell BN hollow spheres with excellent performance in hydrogen storage and wastewater treatment. Energy & Environmental Science, 5(5), 7072-7080.

Liu, D., Cui, W., Lin, J., Xue, Y., Huang, Y., Li, J., . . . Tang, C. (2014). A novel TiO_2− xNx/BN composite photocatalyst: Synthesis, characterization and enhanced photocatalytic activity for Rhodamine B degradation under visible light. Catalysis Communications, 57, 9-13.

Loucks, D. P., & Van Beek, E. (2017). Water resource systems planning and management: An introduction to methods, models, and applications: Springer.

Lowell, S., Shields, J. E., Thomas, M. A., & Thommes, M. (2012). Characterization of porous solids and powders: surface area, pore size and density (Vol. 16): Springer Science & Business Media.

Maniam, G. P., Hindryawati, N., & Yusoff, M. (2015). Rice Husk Silica Supported Oil Palm Fruit Ash as a Catalyst in the Transesterification of Waste Frying Oil. Journal of Engineering and Technology (JET), 6(1), 1-12.

Miao, R., Luo, Z., Zhong, W., Chen, S.-Y., Jiang, T., Dutta, B., . . . Suib, S. L. (2016). Mesoporous TiO_2 modified with carbon quantum dots as a high-performance visible light photocatalyst. Applied Catalysis B: Environmental, 189, 26-38.

Ng, K. H., Lee, C. H., Khan, M. R., & Cheng, C. K. (2016). Photocatalytic degradation of recalcitrant POME waste by using silver doped titania: Photokinetics and scavenging studies. Chemical Engineering Journal, 286, 282-290.

Nichols, J., & Smith, A. (2009). Naive and primed pluripotent states. Cell stem cell, 4(6), 487-492.

Nithin, B. R., Bhuyar, P., Trejo, M., Rahim, M. H. A., Maniam, G. P., Govindan, N. (2020). Culturing of green photosynthetic microalgae (*Chlorella* sp.) using palm oil mill effluent (POME) for future biodiesel production Maejo Int J Energy Environ Commun, 2(1); 1-8.

Ohtani, B., Prieto-Mahaney, O., Li, D., & Abe, R. (2010). What is Degussa (Evonik) P25? Crystalline composition analysis, reconstruction from isolated pure particles and photocatalytic activity test. Journal of Photochemistry and Photobiology A: Chemistry, 216(2-3), 179-182.

Olanders, B., & Steenari, B.-M. (1995). Characterization of ashes from wood and straw. Biomass and Bioenergy, 8(2), 105-115.

Paine, R. T., & Narula, C. K. (1990). Synthetic routes to boron nitride. Chemical Reviews, 90(1), 73-91.

Pal, M., Pal, U., Jiménez, J. M. G. Y., & Pérez-Rodríguez, F. (2012). Effects of crystallization and dopant concentration on the emission behavior of TiO_2: Eu nanophosphors. Nanoscale research letters, 7(1), 1.

Pawari, M., & Gawande, S. (2015). Ground water pollution & its consequence. International journal of engineering research and general science, 3(4), 773-776.

Porter, J. F., Li, Y.-G., & Chan, C. K. (1999). The effect of calcination on the microstructural characteristics and photoreactivity of Degussa P-25 TiO_2. Journal of materials science, 34(7), 1523-1531.

Rehman, S., Ullah, R., Butt, A., & Gohar, N. (2009). Strategies of making TiO_2 and ZnO visible light active. Journal of hazardous materials, 170(2-3), 560-569.

Rusbintardjo, G., Hainin, M. R., & Yusoff, N. I. M. (2013). Fundamental and rheological properties of oil palm fruit ash modified bitumen. Construction and Building Materials, 49, 702-711.

Sarina, S., Waclawik, E. R., & Zhu, H. (2013). Photocatalysis on supported gold and silver nanoparticles under ultraviolet and visible light irradiation. Green Chemistry, 15(7), 1814-1833.

Sing, K. S. (1985). Reporting physisorption data for gas/solid systems with special reference to the determination of surface area and porosity (Recommendations 1984). Pure and applied Chemistry, 57(4), 603-619.

Sun, H., Liu, S., Liu, S., & Wang, S. (2014). A comparative study of reduced graphene oxide modified TiO_2, ZnO and Ta_2O_5 in visible light photocatalytic/photochemical oxidation of methylene blue. Applied Catalysis B: Environmental, 146, 162-168.

Sun, Q., Hu, X., Zheng, S., Sun, Z., Liu, S., & Li, H. (2015). Influence of calcination temperature on the structural, adsorption and photocatalytic properties of TiO_2 nanoparticles supported on natural zeolite. Powder Technology, 274, 88-97.

Tangchirapat, W., Saeting, T., Jaturapitakkul, C., Kiattikomol, K., & Siripanichgorn, A. (2007). Use of waste ash from palm oil industry in concrete. Waste Management, 27(1), 81-88.

Udoetok, I. (2012). Characterization of ash made from oil palm empty fruit bunches (oefb). International Journal of Environmental Sciences, 3(1), 518-524.

Wang, W., Yu, J., Xiang, Q., & Cheng, B. (2012). Enhanced photocatalytic activity of hierarchical macro/mesoporous TiO_2–

graphene composites for photodegradation of acetone in air. Applied Catalysis B: Environmental, 119, 109-116.

Yalçin, Ş., & Mutlu, I. (2012). Structural characterization of some table salt samples by XRD, ICP, FTIR and XRF techniques. Acta Physica Polonica-Series A General Physics, 121(1), 50.

Yaman, S. (2004). Pyrolysis of biomass to produce fuels and chemical feedstocks. Energy conversion and management, 45(5), 651-671.

Yu, Y.-t. (2004). Preparation of nanocrystalline TiO_2-coated coal fly ash and effect of iron oxides in coal fly ash on photocatalytic activity. Powder Technology, 146(1-2), 154-159.

Yuan, H. (2017). Bioelectrochemical Systems: Microbiology, Catalysts, Processes and Applications. Virginia Tech, 5.